Journal of Hydrology 568 (2019) 1017–1030

Contents lists available at ScienceDirect

Journal of Hydrology

journal homepage: www.elsevier.com/locate/jhydrol

Research papers

Water and salt balance modelling of intermittent catchments using a physically-based integrated model

Hossein Daneshmand[a,*], Sina Alaghmand[b], Matteo Camporese[c], Amin Talei[a], Edoardo Daly[b]

[a] School of Engineering, Monash University Malaysia, Bandar Sunway, Malaysia
[b] Department of Civil Engineering, Monash University, Clayton, Australia
[c] Department of Civil, Environmental and Architectural Engineering, University of Padova, Padova, Italy

ARTICLE INFO

This manuscript was handled by Marco Borga, Editor-in-Chief, with the assistance of Anthony Peter O'Grady, Associate Editor

Keywords:
MIKE SHE
Intermittent catchments
Integrated modelling
Groundwater-surface water interaction
Dryland salinity

ABSTRACT

This paper presents a model of flow and solute transport of intermittent catchments in arid and semi-arid regions, highlighting challenges caused by the complex interactions between subsurface and surface flows. A case study is used for the application of the integrated MIKE SHE model to investigate temporal and spatial dynamics of water and salinity in a small ephemeral catchment in southwestern Victoria, Australia. MIKE SHE was successfully calibrated and validated against experimental data of streamflow, groundwater levels, and salt discharged from the catchment. Projections of climatic conditions, adopting Representative Concentration Pathways (RCPs) 4.5, 6.0, and 8.5, were used to infer how salinity discharge and concentrations might be affected across a range of greenhouse gas emission scenarios with different severity. The calibration of the water fluxes was solely based on parameters associated with the model of evapotranspiration, with other parameters selected from field observations and literature. The calibrated parameters for the salt transport were the longitudinal and lateral dispersivities. The calibration and validation of streamflow series led to Index of Agreement (IoA) of 0.92 and 0.8 respectively, while the simulation of groundwater levels was more challenging (IoA ranging from 0.22 to 0.89). Parameter equifinality was observed, with different parameter sets achieving a good fit of streamflow and groundwater levels, although leading to differing spatial patterns of evapotranspiration rates. Calibration and validation of the discharge concentrations appeared more difficult (IoA of 0.35 for calibration and 0.44 for validation) as they are affected by errors in the simulated flow. Climate projections RCP 8.5 suggested a reduction of salt discharge with consequent increased concentrations within the catchment. The study showed the ability of MIKE SHE to be successfully applied to intermittent dry catchments to possibly support water and land management.

1. Introduction

Dryland salinization is a key worldwide issue causing significant economical losses as a result of crop yield decline and damages to infrastructures (Flugel, 1995; Ghassemi et al., 1995; Jolly et al., 2001). About 831 million hectares of land around the world are affected by salinity (Rengasamy, 2002, 2006; Runyan and D'Odorico, 2016). In Australia alone, for example, 83% of the total dryland cropping area is estimated to be affected by either water table-induced or transient salinity (Rengasamy, 2002), with salinity also being a key contributor to progressive degradation of wetlands and rivers (Jolly et al., 2008; Ridley and Pannell, 2006).

Considerable attention has been paid to mechanisms and repercussions of developing saline groundwater caused by land-use change (Lambers, 2003; Marchesini et al., 2017; McFarlane et al., 2016), with many experimental studies dealing with the impacts of restoring land use to deep-rooted perennial pasture or tree plantation (Adelana et al., 2015; Brown et al., 2005; Dean et al., 2016). Because modelling of the water fluxes of catchments in arid and semi-arid regions presents specific challenges, such as the occurrence of substantial periods of no flow, the rapid burst of streamflow following large storms, and possibly the seasonality of runoff generation mechanisms (Pilgrim et al., 1988; Wheater et al., 2007), the development of such models in arid and semi-arid areas is not well established. Models of salt transport in these areas are even rarer, and are often restricted to lumped models (Anderies, 2005; Suweis et al., 2010; Tuteja et al., 2003; Walker et al., 2002). Overall, hydrological models in intermittent catchments are not very common, with most applications relying on lumped descriptions of rainfall runoff processes (Croke et al., 2008; Ye et al., 1997, 1998).

Recently, distributed models for surface and subsurface water fluxes

* Corresponding author.
E-mail address: Hosseindany@gmail.com (H. Daneshmand).

https://doi.org/10.1016/j.jhydrol.2018.11.035
Received 27 February 2018; Received in revised form 13 November 2018; Accepted 14 November 2018
Available online 22 November 2018

have been applied to water flow in intermittent catchments (Camporese et al., 2014; Jiang et al., 2015; Niedda and Pirastru, 2014), with only a few also describing salinity and solute transport (Alaghmand et al., 2014a,b, 2015; Scudeler et al., 2016).

The development of hydrological models able to describe the main dynamics of subsurface-surface water interaction in arid and semi-arid areas, where flow is intermittent, and to simulate the relationships between a suite of stresses, such as water limitations and catchment salinization, is very valuable for catchment management. Projections of future conditions of water fluxes and stores as well as their implications for soil salinity and land productivity are important for water allocation, and are especially challenging for arid environments with large climatic variability (Leblanc et al., 2012). Although projections of climatic trends are very common for atmospheric variables such as temperature and rainfall, the translation of these projections to catchment hydrological conditions and salinization is still rare.

This study thus has two aims. The main aim is to test the ability of a well-established integrated surface–subsurface hydrological model (ISSHM), i.e. MIKE SHE, to simulate water and salt fluxes in intermittent catchments. This is a challenging endeavor considering the complexity of intermittent catchments, where both streamflow and groundwater levels need to be modelled appropriately to be able to reproduce flow periods and magnitudes as well as the associated salt dynamics. The second aim is to show the application of the integrated model in future projections of water and salt balance at the catchment scale, with potential applications to water and land management. Use of ISSHMs for future projections is rare in the literature, and the intent here is not to provide future prediction, but to show that hydrological models that describe a series of complex processes can be effectively used as tools to support catchment management.

2. Materials and methods

2.1. Study site and data description

The study site is a small catchment (0.48 km^2) located at Mirranatwa in southwest Victoria, Australia. The outlet of the catchment is located at an elevation of 254 m above the Australian Height Datum (AHD), with the highest elevation of the catchment being about 305 m (Fig. 1). The catchment is mainly used as rain-fed pasture for grazing sheep with winter active grass cover. The climate falls under Cfb (Mediterranean, maritime/temperate) in the Koppen classification system, with wet winters and springs, and dry summers. In the last 10 years, the mean annual rainfall amounted to 638 mm while annual mean reference evapotranspiration was estimated at 1071 mm using the Hargreaves-Samani method (Hargreaves and Samani, 1985). The ratio between these terms yields an Aridity Index (Barrow, 1992) of 0.59, placing the area in the category of dry-subhumid.

The upper regolith layer is composed of around 7 m of alluvial/colluvial material, underlain by granite, which has decomposed to variable extents, resulting in a decrease in hydraulic conductivity with depth. At 30 m depth, the granite bedrock constitutes a relatively impermeable layer. Further details on the site can be found in Dean et al. (2016) and Dresel et al. (2018).

Catchment discharge was monitored at 30-min intervals using a triangular weir at the catchment outlet (Dean et al., 2016). Daily groundwater levels were calculated from levels in 8 bores (Fig. 1) at 4-h intervals. Electrical conductivity (EC) of the discharge water was available from measurements by a conductivity cell installed at the base of the weir pool. EC in $\mu S\,cm^{-1}$ was internally compensated for temperature and multiplied by a constant factor of 0.6 to estimate Total Dissolved Solids (TDS) in $^{-1}$ (DEDJTR, 2017). Groundwater salinity was available as the concentration of TDS from a composition analysis of groundwater samples in 2010 and 2011 (Dean et al., 2014). However, to be consistent with the discharge measurements, groundwater salinity was also estimated based on EC.

Vapour pressure, temperature and solar radiation data were taken from the Queensland Government SILO spatially interpolated database (http://www.longpaddock.qld.gov.au/silo). Daily rainfall data were from the Bureau of Meteorology (BOM) weather station 089019 located 2 km to the south of the study area. Standardized reference evapotranspiration (ET_o) was obtained through a reduced-set FAO-56 method, which requires wind speed as a long-term average value. Estimations are available as monthly wind speed grids produced from BOM's MesoLAPS PT125 model simulations.

Climate projections were also obtained from the SILO database, available from the Consistent Climate Scenarios project.

2.2. Model selection and description

Five commonly used physically-based Integrated Surface–Subsurface Hydrological models (ISSHMs) were reviewed (Table 1). ParFlow is a parallel, integrated hydrological model that simulates spatially distributed surface and subsurface flow as well as land surface processes including evapotranspiration and snow (Maxwell et al., 2015). The Process-based Adaptive Watershed Simulator (PAWS; Shen and Phanikumar, 2010) describes major hydrologic processes (e.g., surface–subsurface flow, river network, wetlands, vegetation and snowpack) using an efficient surface–subsurface coupling scheme. These two models currently do not model surface and subsurface solute

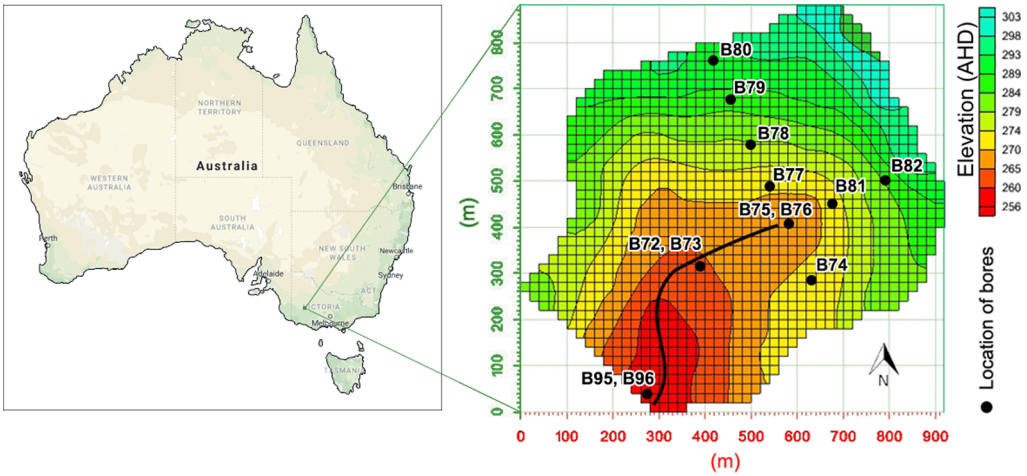

Fig. 1. Left: catchment location within Australia. Right: catchment digital elevation model with the creek shown as a black line. Dots and numbers identify the network of groundwater bores. B72, B73, B77, B79, and B81 only have EC measurements and other bores have both water level and EC measurements.

Table 1
ISSHMs reviewed for consideration for this study.

ISSHM	Surface flow	Subsurface flow	Surface transport	Subsurface transport	Vegetation model
ParFlow	2D kinematic wave	3D Richards	N/A	Advection, decay, sorption	Coupled to CLM
PAWS	2D Diffusive-wave	1D Richards coupled to Quasi 3D Darcy	N/A	N/A	Representative Plant type
Cathy	1D kinematic wave	3D Richards	A/D	A/D	Feddes
HGS	2-D diffusive-wave	3D Richards	A/D	A/D, decay, sorption	K&J
MIKE SHE	2D Diffusive-wave	1D Richards coupled to 3D Darcy	A/D	A/D, decay, sorption, particle tracking	K&J

A/D: Advection/Diffusion; K&J: Kristensen and Jensen, 1975 evapotranspiration model; N/A: Not Applicable; CLM: Community Land Model.

transport. Catchment Hydrology (CATHY) and HydroGeoSphere (HGS) couple a three-dimensional equation for subsurface flow to approximations of the Saint Venant equation for surface flow, and they have been used for both water fluxes and solute transport (Alaghmand et al., 2016; Haaken et al., 2017; Liggett et al., 2014; Scudeler et al., 2016). MIKE SHE is also capable of modelling water fluxes and solute transport (e.g., Hester et al., 2016; Long et al., 2015).

For surface flow, all the models solve a 2D representation of surface flow except CATHY, which implements an algorithm to define a network of 1D flow paths (Camporese et al., 2010). For the subsurface, PAWS and MIKE SHE benefit from higher computational efficiency due to a lower dimensionality in the non-linear Richards' equation. The models are thus better applicable to catchment-scale problems, where lateral fluxes are small compared to vertical fluxes in the unsaturated zone (Kollet et al., 2016). Advection and diffusion are the main processes defining the transport of salt in both surface and subsurface. These two are included in three of the models; however, some also implement other processes, such as decay and sorption, which are applicable to other solutes. ParFlow could be coupled to the Community Land Model (CLM; Oleson et al., 2008) to provide evapotranspiration as well as other processes (Kollet and Maxwell, 2006), while MIKE SHE and HGS use the method developed by Kristensen and Jensen (1975), and CATHY can implement either a boundary condition switching procedure or root water uptake formulations (Camporese et al., 2015). A comparison of performance for these models can be found in Maxwell et al. (2014) and Kollet et al. (2016).

MIKE SHE was selected for this study because it is designed for simulations of both water and solute fluxes at the catchment scale, and uses a very computationally efficient coupling between the saturated and unsaturated zone models.

Details of MIKE SHE are in DHI (2014) and a brief summary is provided here. The subsurface model is composed of two separate modules for the saturated and unsaturated zones. Flow in the saturated zone is described by the three-dimensional Darcy equation, while the flow in the unsaturated zone is described by the one-dimensional Richards equation (Richards, 1931). The flow equation in the unsaturated zone is coupled to the saturated zone at the interface via a pressure boundary condition, thereby allowing for larger times for the saturated flow. Surface runoff is modelled as a two-dimensional, sheet flow using the diffusive wave approximation of the Saint Venant equations and a Strickler/Manning-type law to relate flow depth to velocity (Chanson, 2004).

Solute transport is modelled with an advection–dispersion equation coupled to overland flow and the flow in the saturated and unsaturated zones. In the subsurface, dispersion is controlled by longitudinal and transverse dispersivities (α_L, α_T), while in the overland flow there is no general relationship between the mean flow velocity and dispersion, and thus the dispersion coefficient (D) needs to be specified directly.

The value of actual evapotranspiration is calculated at each grid cell dynamically, described as the sum of three individual components, namely actual transpiration (E_{at}), evaporation from the soil surface (E_s), and direct evaporation from vegetation canopy (E_{can}). At each time step, E_{at} is calculated as a fraction of the reference evapotranspiration (ET_o) depending on soil moisture, vegetation and other soil attributes (Kristensen and Jensen, 1975); E_{at} is thus calculated from the root extinction depth as

$$E_{at} = f_1(LAI)\cdot f_2(\theta)\cdot f_3(A_{root}, Z_r)\cdot ET_o, \quad (1)$$

where f_1 accounts for a reduction of root uptake depending on Leaf Area Index (LAI), f_2 limits the root uptake based on soil saturation, θ, and f_3 is the root distribution function (RDF), which is described in terms of a root shape factor (A_{root}) and root extinction depth (Z_r). The equation for soil evaporation is

$$E_s = ET_o\cdot f_4(\theta) + [ET_o - E_{at} - ET_o\cdot f_4(\theta)]\cdot f_5(\theta)\cdot[1 - f_1(LAI)], \quad (2)$$

where the first term on the right-hand side ($ET_o\cdot f_4(\theta)$) describes multiple phases of a persistent evaporation from soil surface depending on soil moisture content, and the second term describes soil evaporation when soil moisture approaches field capacity (DHI, 2014; Kristensen and Jensen, 1975).

The evaporation from vegetation canopy is obtained as

$$E_{can} = min(I_{max}, ET_o\cdot\Delta t), \quad (3)$$

where Δt is the model time step, and I_{max} is the maximum canopy storage defined as

$$I_{max} = C_{int}\cdot LAI, \quad (4)$$

C_{int} being the canopy interception coefficient.

2.3. Model set up

2.3.1. Model parameters

The average specific yield of the aquifer as well as values of some of the parameters characterizing the soil according to the Van Genuchten retention curve formulation (Van Genuchten, 1980) are calibrated values from a model presented in Camporese et al. (2014) and Dean et al. (2016) based on a grain size analysis reported in Dean et al. (2015). Due to the small size of the catchment, subsurface parameters were assumed constant across the catchment. The saturated hydraulic conductivity was assumed to decrease with depth according to $K_s = 1.01 \times 10^{-5} z^{-0.27}$ (Camporese et al., 2014; Dean et al., 2016). Porosity (θ_s) was given an average value of 0.40 and specific yield was assigned the mean value of measurements at 0.095 ± 0.014 (Dean et al., 2015). Saturation at field capacity (θ_{fc}) and water content at wilting point (θ_{wp}) were calculated using the Van Genuchten curve at 0.3 and 0.05 corresponding to suction pressures of 0.0061 and 1.5538 MPa, respectively. Specific storage coefficient (S_s) was found to be an insensitive parameter; therefore, a value of 1×10^{-3} m^{-1} was assigned uniformly across the catchment. The key parameters in the Kristensen and Jensen, 1975 model are $C1$, $C2$, and LAI. Acceptable ranges taken from the literature (Vazquez, 2003) were used in an auto-calibration procedure. Parameter $C3$ was given the value of 20 mm day^{-1}, while canopy storage was assigned a typical value of 0.2 mm as no sensitivity was observed for feasible values of this parameter. To limit root water uptake to the first 20 cm of the soil column, representing annual pasture grass, a constant value of 1 m^{-1} was assigned as A_{root}, and root extinction depth was set equal to 1 m. The solute transport model parameters α_L and α_T were obtained through model calibration, while D in the surface flow was neglected due to insensitivity. All parameters used in this study and their values are listed in Table 2.

Table 2
Main parameters characterizing the soil, surface flow, transpiration (K&J stands for Kristensen and Jensen, 1975), and solute transport.

Parameter	Value
Saturated hydraulic conductivity (K_s)	$K_s = 1.01 \times 10^{-5} z^{-0.27}$ [m s^{-1}]
Specific storage (S_s)	1×10^{-3}[1 m^{-1}]
Specific yield (S_y)	0.095
Saturated water content (θ_s)	0.4
Moisture content at field capacity (θ_{fc})	0.309
Wilting point (θ_{wp})	0.049
Residual moisture content (θ_r)	0.03
Matric potential at field capacity (ψ_{fc})	0.0061 MPa
Matric potential at wilting point (ψ_{wp})	1.5538 MPa
Van Genuchten α	1.85[m^{-1}]
Van Genuchten n	1.52
Manning number channel (m)	10[m$^{1/3}$ s^{-1}]
Manning number slope (m)	1[m$^{1/3}$ s^{-1}]
K&J LAI*	1.01
K&J $C1$*	0.34
K&J $C2$*	0.4
K&J $C3$	20 [mm day^{-1}]
K&J Root Extinction Depth (Z_r)	1 [m]
Root distribution factor (A_{root})	1[m^{-1}]
Canopy storage coefficient (C_{int})	0.2 [mm]
Longitudinal Dispersivity (α_L*)	5 [m]
Transverse Dispersivity (α_T*)	0.5 [m]
Dispersion Coefficient (D*)	0 [m^2 s^{-1}]

* Parameter values obtained through calibration

2.3.2. Discretization

The model grid was constructed from a digital elevation model with a 20 m x 20 m cell resolution. The vertical discretization for the unsaturated zone consisted of 16 layers of exponentially increasing thickness, beginning from 0.05 m near the surface and ending at 2 m. For the saturated zone, an initial simulation using a single soil layer was first performed to approximately obtain the minimum water table levels required to minimize errors associated with the coupling of saturated and unsaturated zones (DHI, 2014). The elevation map of the minimum water table depths was then used to define the bottom slice of the first saturated layer, while the remaining thickness up to the bottom model domain boundary was evenly divided to provide, overall, five saturated-zone layers.

2.3.3. Boundary conditions

Based on a significant reduction in hydraulic conductivity with depth, an impermeable bottom boundary was assumed 10 m below the ground surface. All the lateral boundaries of the catchment were also assumed impermeable (Dean et al., 2016), and daily rainfall and evapotranspiration defined the flux boundary condition at the soil surface.

The boundary conditions for the solute transport equation were defined based on primary sources of salt and their measurements reported in Dean et al. (2014). One of these identified sources is dissolved salts in rainwater, for which measurements indicate a mean value of 7 mg l^{-1}; this value was used to impose a flux boundary condition at the soil surface where the mass input of salt is determined by the rainfall volume. To obtain an estimation for the rate of salt input through decomposition of granite material, which is another continuous source of salt, the average annual salt input from rainfall was multiplied by the ratio between granite-originated and rainfall-originated solute concentrations. The obtained value (0.64 tonne year^{-1}) was then assigned as a prescribed salts flux boundary condition to the bottom layer.

2.3.4. Initial conditions

A recursive simulation (Ajami et al., 2015) showed that the shortest time for the system to reach a status not affected by the initial conditions is achieved when the warm-up run starts from soil moisture at field capacity across the catchment. To minimize model sensitivity to the initial conditions, starting from soil moisture at field capacity, 10 years of real precipitation, solar radiation, and minimum and maximum daily temperature data were used in a warm-up run. This includes the majority of the Millennium Drought period (i.e., 1996 to 2009; van Dijk et al., 2013) to ensure that the modelled catchment conditions are physically consistent and properly reflect the history of the catchment. The final catchment state resulting from this simulation was used as initial condition to start the calibration run.

The initial conditions for the solute transport model were defined based on the groundwater salinity measurements, whose current levels are reported to be due to the deposition of salts from rainwater over time and decomposition of the bedrock prior to land-use change (Dean et al., 2014). For initial groundwater salt concentrations, a raster map approximating salinity at each grid cell was required. Since the number of sampling bores was not adequate to perform interpolation, this was achieved using an observed relationship between surface elevation and groundwater TDS. To this end, observed salinities for the bores (Dean et al., 2014) were plotted against the surface elevation at these bores. Samples from B77 and B80 (See Fig. 1) were excluded in this relationship, because B77 receives freshwater through preferential pathways along the granite fractures (Dean et al., 2014), and B80 reaches the deep aquifer below the model domain. A linear decrease in salinity with increasing ground surface elevation was observed with a coefficient of determination equal to 0.85 (Fig. 2). The progressive addition of salt to groundwater from infiltration causes a gradual increase of groundwater salinity towards the lower parts of the catchment (e.g., Bennetts et al., 2006).

Salt concentration measurements in the unsaturated zone were not available, thus the model was used to infer their initial value. In the unsaturated zone, the model produced quick salinity levels in equilibrium with the groundwater. The model was run for several years repeating climatic data from one year before the actual simulation period (i.e., year 2010), with the observed concentrations of groundwater imposed as a constant concentration boundary condition in the saturated zone layers. Given the estimated distribution of groundwater salinity, the salinity of the unsaturated zone approached a common value at the end of each year across the catchment, indicating no sensitivity of the concentration distribution in the unsaturated zone to the number of initialization years. Therefore, this common distribution was used as the initial concentration (Fig. 2c). Any possible storage of salt in the deep regolith can be reasonably assumed to be immobile, considering that the clearance of the native vegetation cover has occurred more than a century ago, and hence the aquifer has been under recharge ever since (White et al., 2003).

2.4. Calibration and validation

Most of the model parameters were estimated from field measurements and previous modelling work of the water balance at the same catchment (Camporese et al., 2014; Dean et al., 2016). Vegetation specific parameters and diffusive transport parameters (i.e., longitudinal and transverse dispersivities as well as surface flow dispersion coefficient) were obtained through calibration (Table 2). A preliminary sensitivity analysis revealed that the determining parameters in controlling evapotranspiration are $C1$, $C2$, and LAI. Therefore, feasible ranges of these parameters were taken from the literature for an auto-calibration procedure (Vazquez, 2003).

The Population Simplex Evolution algorithm, implemented in the AUTOCAL software (Madsen, 2003), proved to be efficient, and was thus used for auto-calibration. The period chosen for model calibration was the time interval of 15–02-2011 to 15–02-2012, while the subsequent year, from 16–02-2012 to 15–02-2013, was chosen as the model validation period. The Root Mean Square Error (RMSE) between observed and simulated values of streamflow was the calibration

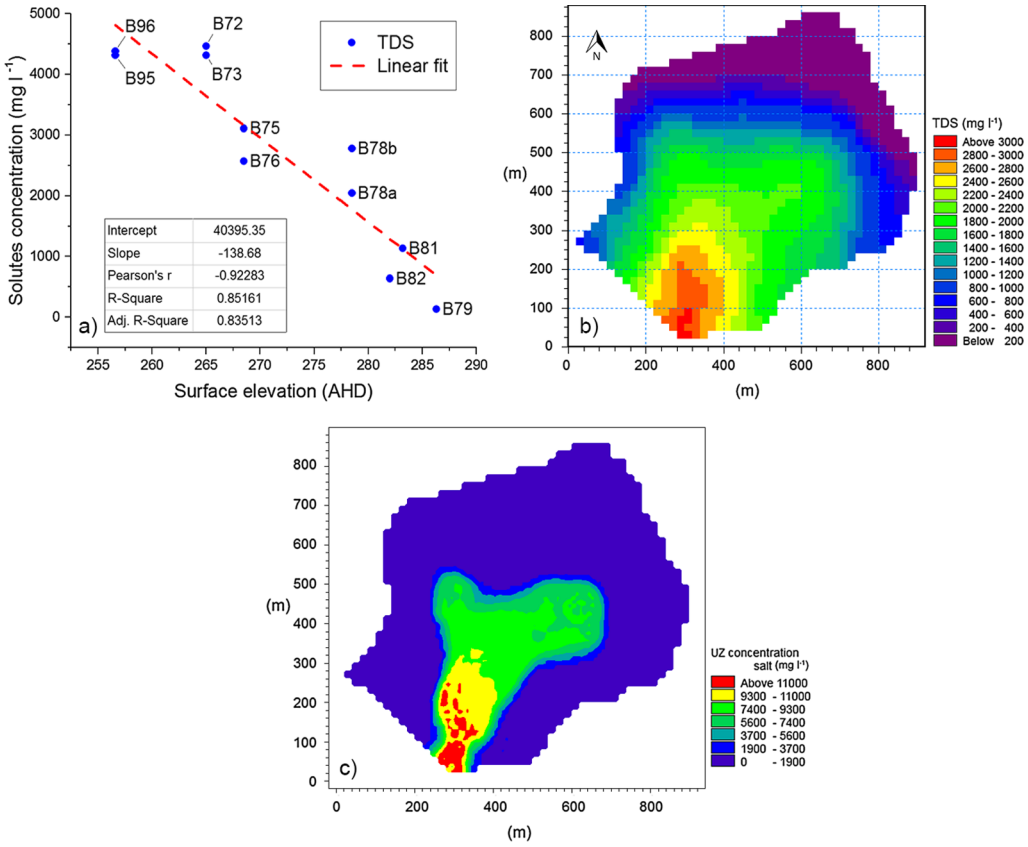

Fig. 2. Panel a: Concentration of Total Dissolved Solids (TDS) in groundwater as a function of surface elevation at sampling points in 2010 and 2011 (data from Dean et al., 2014). Panel b: The groundwater salinity map obtained from the linear relationship. Panel c: Initial salt concentrations in the unsaturated zone at a cross Section 1 m below the surface.

objective function. Other metrics, such as the Index of Agreement (IoA; Willmott, 1981) and the coefficient of determination (R^2), were also used for the assessment of fit of groundwater levels. As in Camporese et al. (2014) and Dean et al. (2016), the bores considered for the model performance are B76, B74, and B96. With the exception of B95, the other bores had groundwater levels below 10 m, outside the model domain. Although B95 at the outlet has water levels within 10 m from the surface, it is about 30 m deep and screened in the granite bedrock.

Once the flow model results were validated, the solute transport model was calibrated using an iterative trial-and-error method where, in each iteration, the performance of the solute transport model was evaluated by comparing IoA for simulated and the observed concentration values. However, only concentration of the catchment discharge water was used for calibration, since recurrent measurements for groundwater concentration at various bores were not available.

2.5. Projections of climatic conditions

The validated model was used to provide projections in the future status of catchment salinity over a predicted hotter and drier climate using daily weather data projections. These weather projections represent three main greenhouse gas emission scenarios (i.e., RCP 4.5, RCP 6.0, and RCP 8.5) simulated by a General Circulation Model (GCM) in terms of precipitation, solar radiation, minimum, and maximum daily temperature.

For Australia, daily-scaled projections using the Change Factor Method (CFM; Anandhi et al., 2011) are available from the SILO database. This method calculated the arithmetic difference between daily temperature derived from a current (baseline) climate simulation and derived from a future climate scenario taken at the same GCM grid location. This difference was added to historical local values to obtain the modeled future values of daily temperature. For rainfall and solar radiation, multiplicative change factors rather than arithmetic differences between the future and baseline GCM simulations were calculated, and the historical values were multiplied by the change factor. The duration of 1960 to 2015 defined the historical (observed) as well as the baseline (GCM simulated) period, while 2050 was the future scenario year (Queensland Department of Science, Information Technology and Innovation, 2015).

Projected rainfall timeseries were directly used in this study, whereas the projections for other variables were used to estimate the reference evapotranspiration according to the Hargreaves-Samani method. These projections are generated by the CSIRO-MK36, which is among the GCMs reported in the Intergovernmental Panel on Climate Change (IPCC) Fourth Assessment, deemed to be most reliable for the Australian region (Suppiah et al., 2007). A seasonal summary of these projections is given in Table 3.

3. Results and discussion

3.1. Hydrological model

3.1.1. Model performance

Catchment discharge flow for the calibration period is shown in Fig. 3 with water-table levels at three shallow bores near the drainage line, where the water table is more dynamic. Fig. 3 shows that, for the catchment discharge series, the model achieved a good fit (IoA = 0.92) through calibration of only ET parameters. The intermittent regime of flow and timing of events are accurately reproduced, with magnitudes of individual events as well as cumulative discharge being also in good agreement with observations (Fig. 3, inset). Low flow events, in particular during the initial part of the year (February - April) are well captured by the model, indicating a good approximation of initial soil moisture during the warm-up run.

Water-table fluctuations at B96 near the catchment outlet are in agreement with observations in terms of both magnitude and seasonal dynamics, with slight over- and under-estimations during the dry and wet seasons. Water-table levels at B74 follow the seasonal pattern of the

Table 3
Seasonal summary of precipitation projected by CSIRO-MK36 and calculated reference evapotranspiration for 2050.

			RCP 4.5		RCP 6.0		RCP 8.5	
Season	Base P	Base ET_o	P	ET_o	P	ET_o	P	ET_o
J-F-M	99.51	390.55	80.1	405.15	82.3	403.33	75.9	408.8
A-M-J	174.54	129.58	155.9	136.88	158	135.96	151.9	138.7
J-A-S	234.81	143.26	211.5	151.48	214.2	150.56	206.5	153.3
O-N-D	168.78	351.31	140.3	368.65	143.6	366.83	134.1	372.3
Annual	677.64	1014.7	587.8	1062.16	598.1	1056.68	568.4	1073.1

Note: water balance components are given in mm (i.e., volume divided by catchment area).

observations ($R^2 = 0.81$) with an offset of about 2 m throughout the calibration period. Water-table levels at B76 show acceptable consistency with observations during the wet season, when the surface flow maintains the groundwater head at the ground surface.

Similar to the calibration phase, the model is also able to predict the period of flow and the dynamics of groundwater levels for the validation period (Fig. 4). Nevertheless, the annual flow is underestimated and the sharp increase of the water table level near the outlet is modelled as a gradual groundwater rise. It is rather difficult to find a set of parameters that work for an unusually wet year (2011) and a moderately dry year (2012). Considering the challenging nature of arid and semi-arid catchment modelling, it is a good fit for a catchment with a ratio of discharge to rainfall as little as 3%. The performance in both calibration and validation is comparable to previous modelling results in the same catchment (Camporese et al., 2014; Dean et al., 2016). A summary of the model performance for calibration and validation is reported in Appendix A.

3.1.2. Sensitivity analysis

Because three parameters were calibrated, different sets of values of these parameters led to comparable results. To understand how the model responds to these parameters, the parameter sets obtained from auto-calibration were sorted in a table based on RMSE of catchment discharge (see Appendix B). From these parameter sets, those associated with the smallest RMSE values and with little correlation among them were used in individual simulations for the assessment of their control.

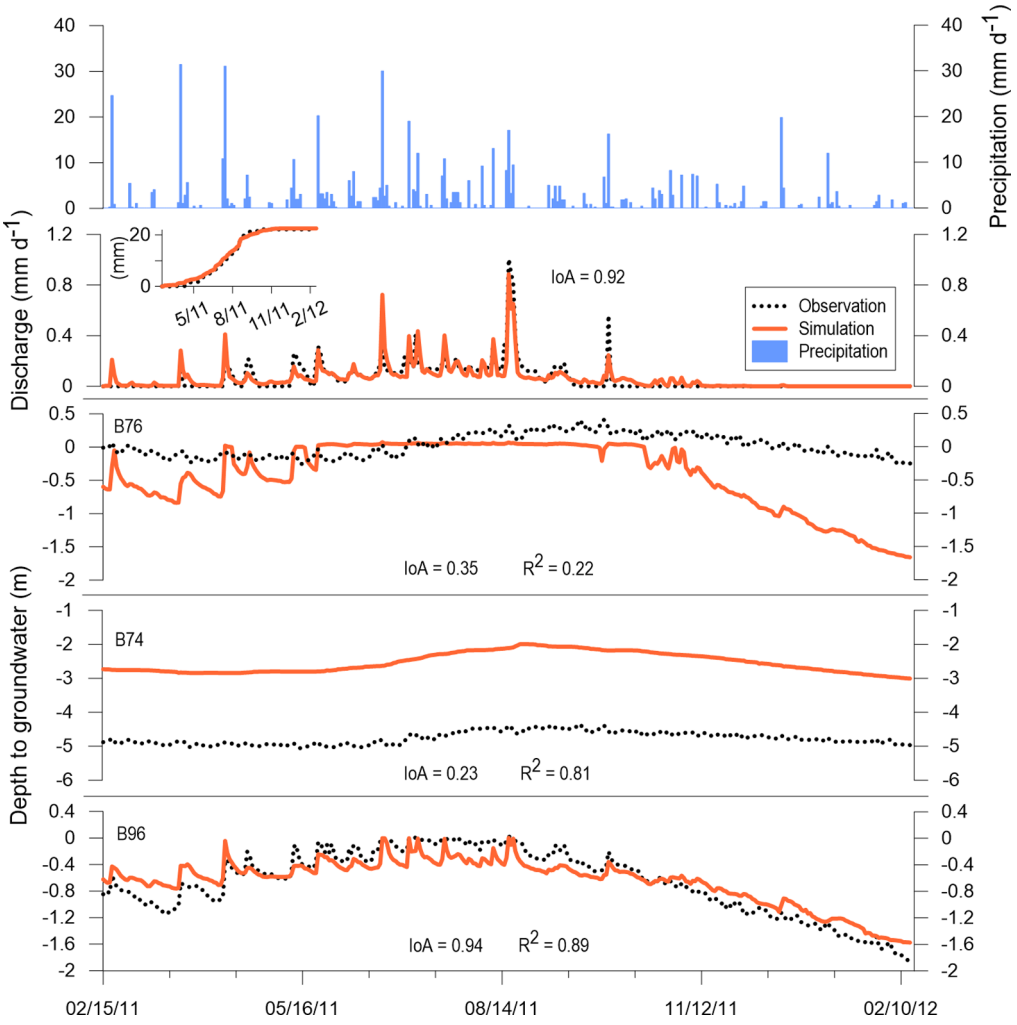

Fig. 3. The hydrological model's calibration results for the year 2011. Measured daily rainfall is shown as blue bars.

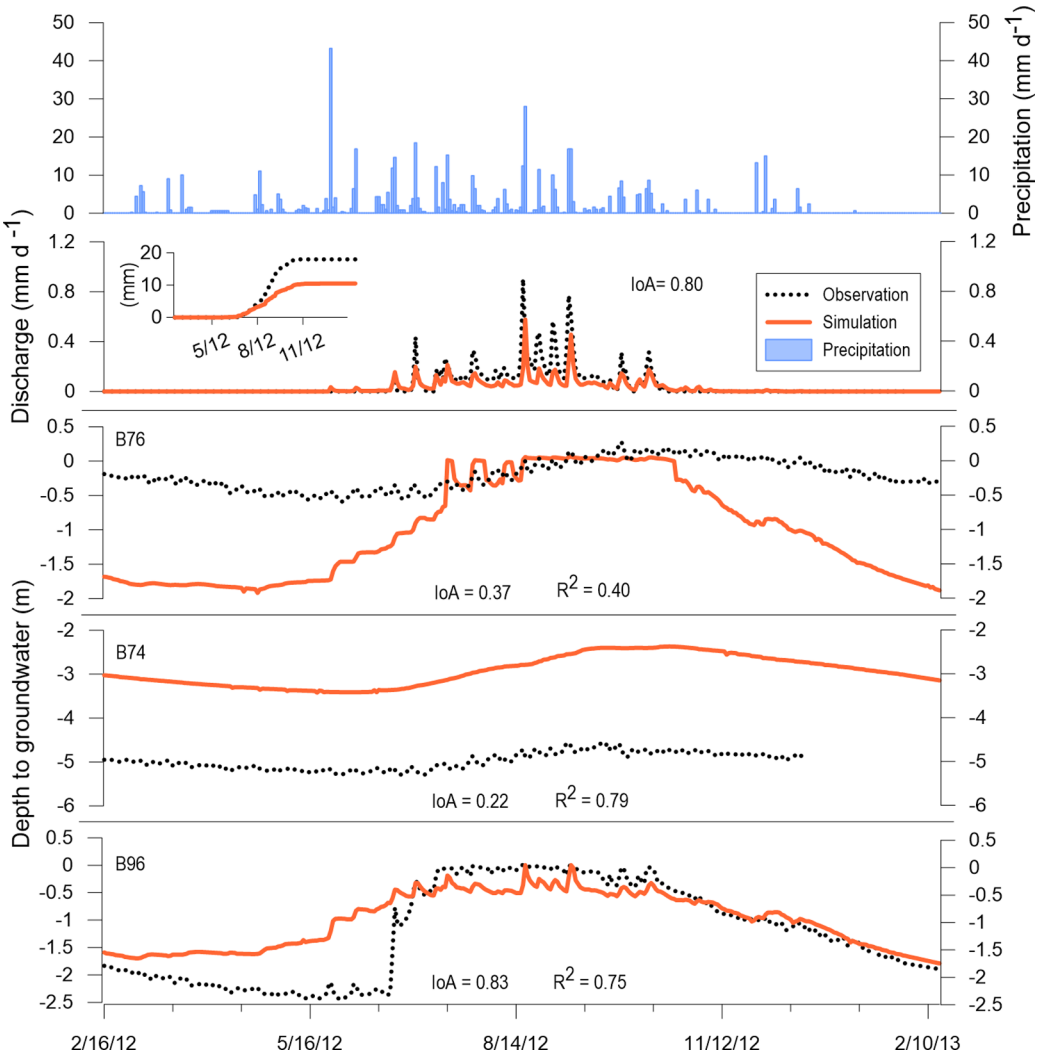

Fig. 4. The hydrological model's validation results for the year 2012.

For all these simulations, equifinality of results was observed for the annual sum of ET and its daily dynamics as well as the water table level in all observation bores; however, as expected, variations were present for the proportionality between ET components as well as the spatial distribution of annual ET.

A quantification of these variations can be obtained by calculating sensitivities of annual E to T ratio (E/T) and absolute annual ET at the location of three observation bores in terms of standardized percentage change. This index can be defined as the variation from the central value of each parameter range at each particular run, divided by the total variation range of that parameter. Fig. 5 shows sensitivities to $C2$ and to the product of LAI and $C1$. The rationale for choosing this product is that the results show no sensitivity to each individual parameter. This is because the product of these two parameters mostly appears in the K&J (Kristensen and Jensen, 1975) formulations with the exception of evaporation from vegetation canopy. This product will be referred to as the vegetation density factor.

Fig. 5 shows the sensitivity of E/T ratio to $C2$ and the vegetation density factor. Considering a similar range of variation for $C2$ and the vegetation density factor (0.31–0.41, 0.34–0.43), it is apparent that equal and opposite variations of the two parameters linearly change E/T, while the total annual ET remains approximately constant. The spatial distribution of annual ET, on the other hand, is considerably affected and its sensitivity differs from point to point. The parameters exhibit a strong complementary control on localized total ET along the drainage line (B76), being less influential at B74 and B96 (Fig. 5). It is possible that the dynamics at B74 and B96 are influenced by the boundary conditions, thereby reducing the effect of changes in the parameters.

Therefore, while the combination of multiple parameters lead to good model performance, dynamics within the catchment can be very different.

3.2. Solute transport model

The calibration of the transport model provided the values 5 m and 0.5 m for α_L and α_T, respectively. Physically realistic values for D did not affect the transport simulation results and, therefore, this parameter was set to zero. Fig. 6 shows the results of the transport model calibration and validation in terms of catchment discharge concentration. For the calibration period, the model is able to reproduce the pattern for individual rainfall events. Concentration match is particularly good for the high flow events between June and September, when the pattern for concentration generally shows marked decreases with rainfall events. The main difference in the measured and modelled concentrations is towards the end of the year, when the stream stops flowing. These differences are mainly caused by the results from the water flow model. Small flow events are modelled in November (see Figs. 3 and 4), while the data did not record any flow event. Therefore, the measured outflow concentrations after early November are zero, while the

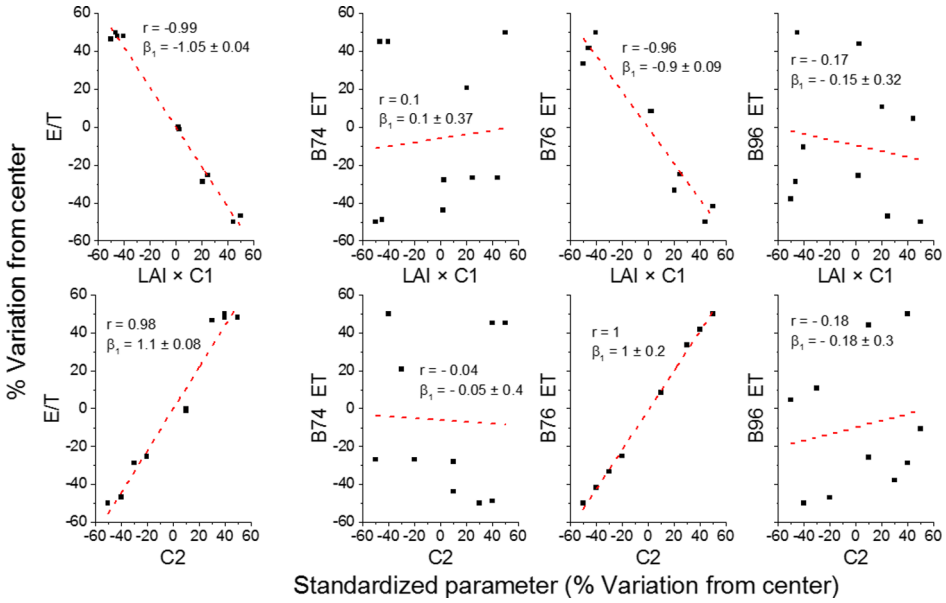

Fig. 5. Sensitivity analysis of total evaporation to transpiration ratio (1st column on the left) and total ET at multiple locations (3 columns on the right) to changes of vegetation density per area (i.e., product of *LAI* and *C*1; top row) and the parameter *C*2 (bottom row).

modelled concentrations are large, because of the very low flow and the already increasing salinity due to the onset of evapotranspiration in spring (September and October). When combined with the water discharge (Figs. 3 and 4), the modelled loads of solute discharged by the catchment are close to those estimated from data during the calibration (2011, inset of Fig. 6a), while the model underestimated the annual discharge in the validation period (2012, inset of Fig. 6b).

Fig. 7 shows salt mobilization dynamics at a point near the catchment outlet for the duration of calibration (top panel) and validation (bottom panel). Salinity is visualized using a color scale over the soil

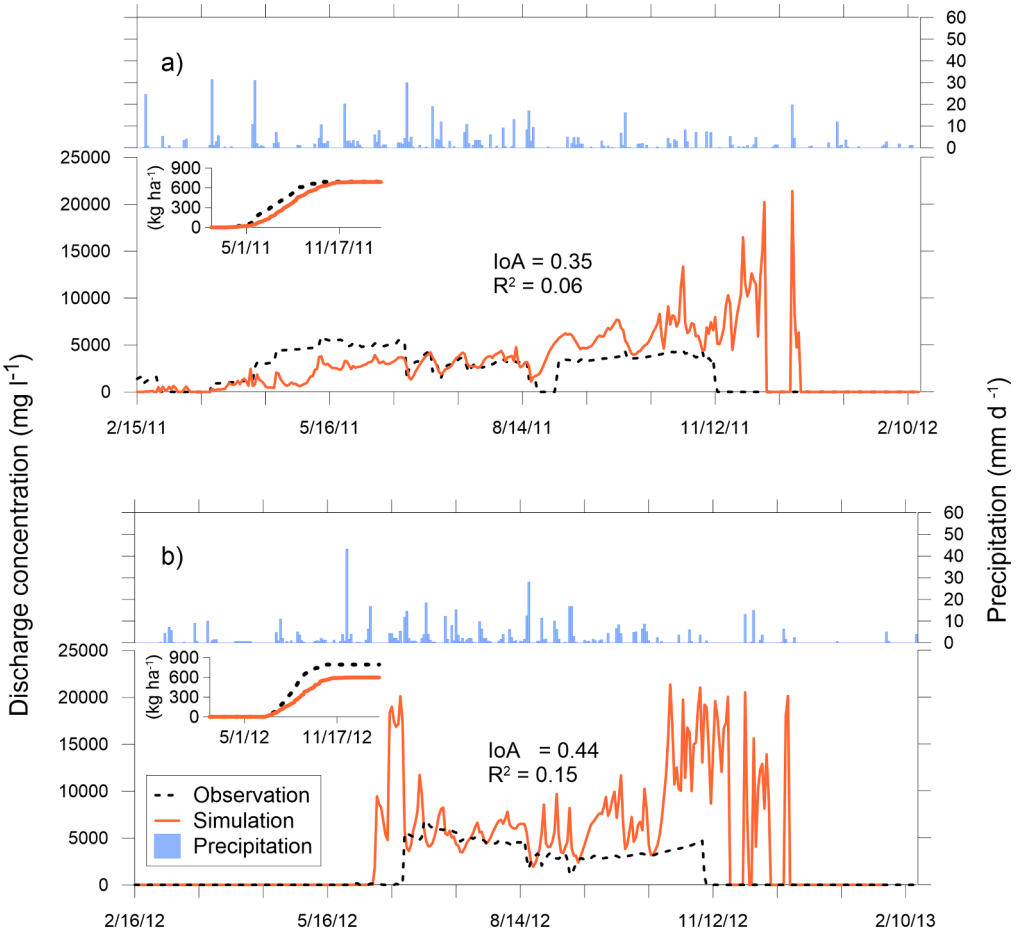

Fig. 6. Calibration (year 2011) and validation (year 2012) of the discharge concentration from the catchment.

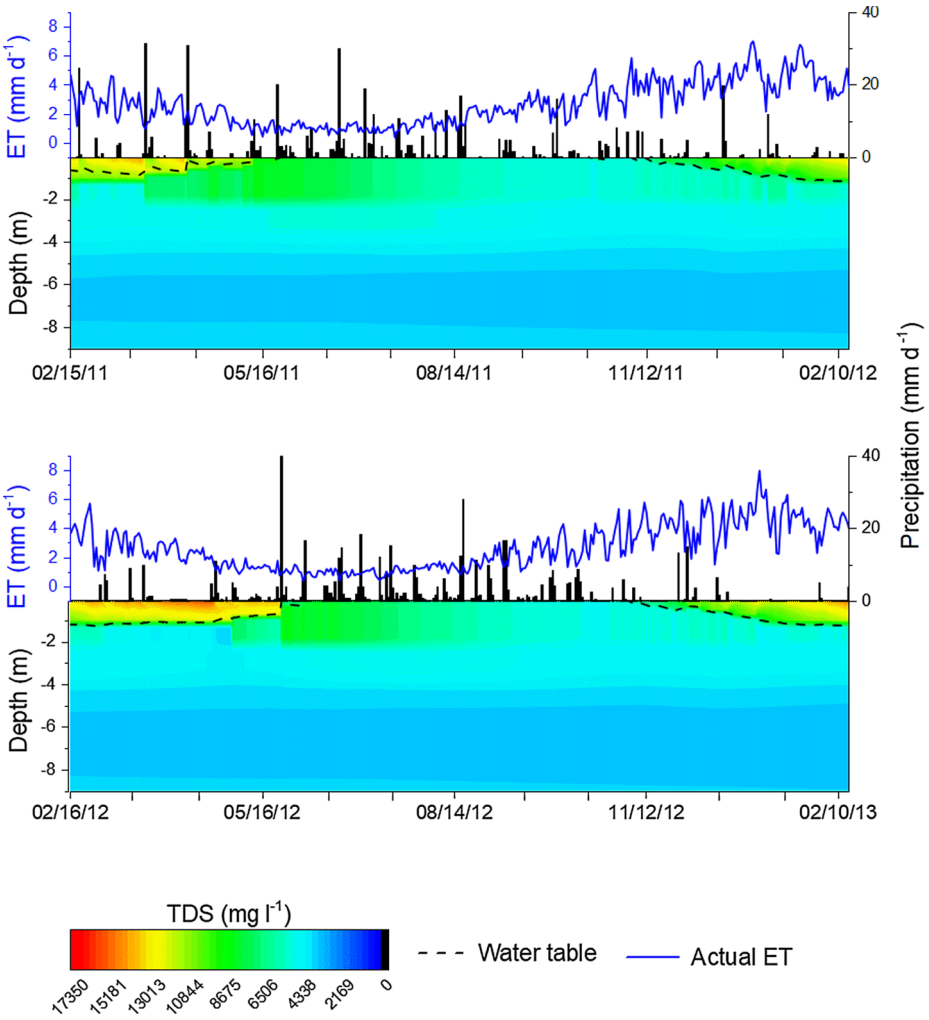

Fig. 7. Salt mobilization dynamics at a point near the catchment outlet with rainfall and ET values.

column along with rainfall and simulated actual ET at this point. This demonstrates the pronounced interactions between the groundwater and the unsaturated zone.

For both calibration and validation periods, a rise in the top-layer groundwater salinity is visible with the start of intensive rainfall events, caused by a leaching of unsaturated storage of salt to the groundwater. However, thereafter groundwater concentration seems to experience a gradual decrease proportionate to discharge flow, hence the solute transport rate. As the water table falls below the ground surface, moisture loss by evapotranspiration results in a capillary flow that is sustained by a subsequent replenishment of moisture from the water table. At this point, due to the proximity of the phreatic surface to the root zone and the high reference evapotranspiration rate, salinization of the top soil occurs at the highest rate. During the dry season, when rainfall fluxes are not large enough to cause groundwater recharge in excess of soil moisture deficit and evapotranspiration rate, transport remains limited to the unsaturated portion of the soil column, reflected as evened out concentration profiles or localized dilution effects commonly observable before the start of diffuse recharge events around April-May.

The model seems to be able to capture the dynamics of solute transport between the saturated and unsaturated zones, with a general rise in unsaturated soil salinity, in the dry season and in groundwater salinity in the wet season. A similar pattern is also visible for total area affected by salinity which reduces during the wet season (see Appendix C). The large depth of the top saturated-zone discretization layer, however, seems to be responsible for some numerically induced dispersion which is recognizable from the larger concentrations in the first layer compared to the second layer and layers below it (Fig. 7). It is, nevertheless, an inevitable requirement of coupling (DHI, 2014) for the top layer to include the phreatic surface.

3.3. Climate change impacts

Simulated results for future salinity in the catchment for three RCP scenarios and a baseline scenario are illustrated in Fig. 8. These results were obtained from the simulation of flow and transport using 56 years of climate projections.

Fig. 8a shows the cumulative salt output versus time. The export rate of salts is consistently the largest under the baseline scenario for the entire simulation duration with a surge occurring near the 50th year, corresponding to an increase in rainfall at the end of the Millennium Drought (i.e., from 1996 to 2009). However, all the RCP scenarios show a significant reduction in the export of salts by the 36th year, which marks the start of a reproduced drought period in the projections. Scenario RCP 8.5 shows a total cessation of salt output from this point onward due to the drying out of the stream.

The drying out of the stream, on the other hand, seems to cause the average salt concentration in unsaturated soil to increase, and is particularly pronounced for RCP 8.5 (Fig. 8b). It is also evident that the salinity of the unsaturated zone is increasing among all RCPs prior to 10 years of simulation. This is due to a fast increase in the salinity of shallow groundwater as a result of evaporative enrichment of transported salt from across the catchment to these low-lying areas. After

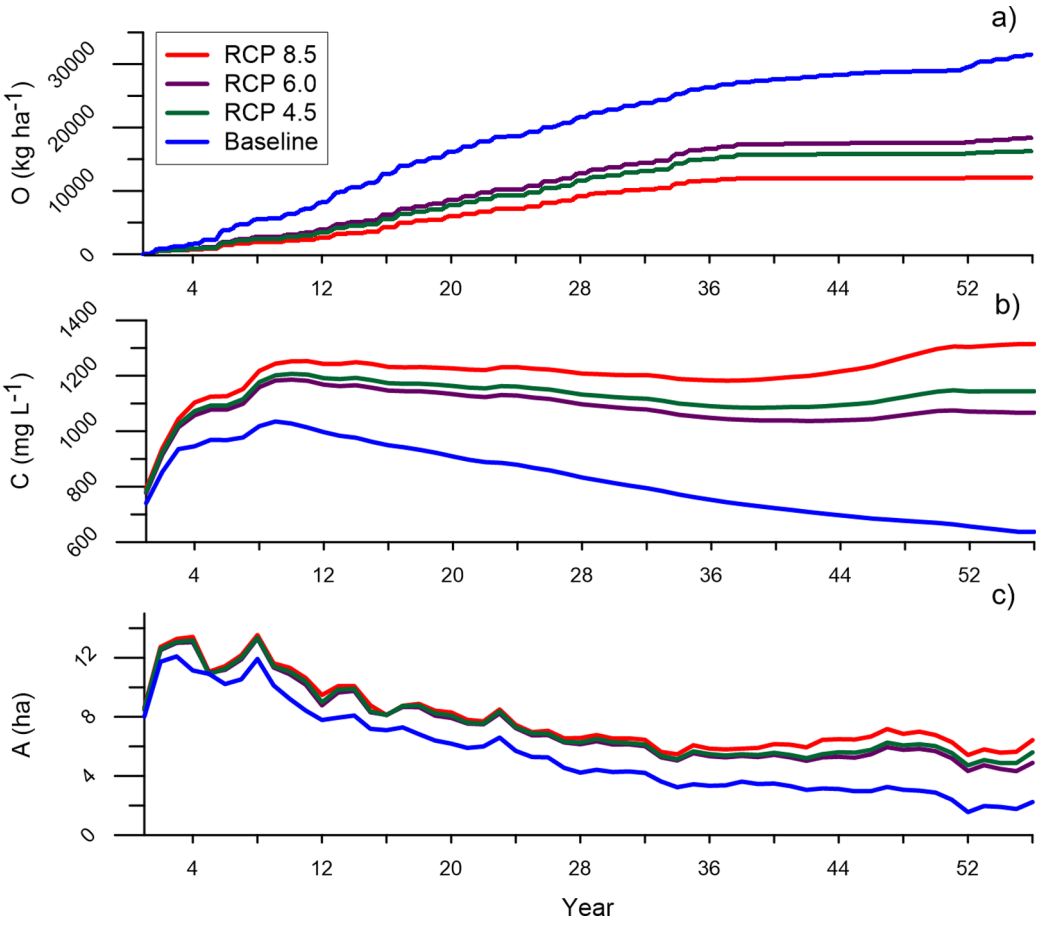

Fig. 8. Results for long term simulation of catchment transport model under RCPs in terms of cumulative salt output (panel a), average concentration of unsaturated soil (panel b), and total area with soil salt concentration above 2000 mg l^{-1} (panel c).

around the 10th year, a drop in the concentration of salt in the groundwater near the outlet will result in reducing salt concentration in the unsaturated zone above groundwater.

The decrease of soil salinity in the unsaturated zone for the baseline climate regime (blue line in Fig. 8b) is associated with the rate of salt output (i.e., salt washed off), which is highest for this scenario because of a larger recharge. As salt leaves the catchment at a faster rate, the overall concentration of both groundwater and top soil decreases faster. In comparison, the other scenarios experience an increase of ET and a reduction in the precipitation amount (Table 3). These cause a lower soil water content, and thus a higher soil salinity; in addition, the lower rainfall means a slower transport, and consequently, a slower depletion of salts, which leads to a sustained groundwater salt concentration. A combination of these two causes provides the obtained effect, which varies in intensity across the scenarios. Historical depletion of groundwater salts due to an output to input ratio larger than one has been documented for the southern half of the Murray-Darling Basin. The rate of this depletion has been shown to decrease with time (Jolly et al., 2001).

Fig. 8c shows the dynamics of the total area that is considered as salt affected (i.e., with a soil salt concentration above 2000 mg l^{-1}). The general pattern is decreasing among all RCPs as well as for the baseline scenario. No significant variation of results is noticeable among the RCPs except during and after the drought period when RCP 8.5 shows a marked divergence from other RCPs.

Overall, the three variables show considerably different projections across the climate scenarios. Scenario RCP 8.5, which is associated with extreme greenhouse gas emissions, exhibits the utmost deviation from the baseline scenario with total output of salt at the end of this period reduced to nearly half compared to the baseline. Under all climate change scenarios, average soil salinity remains relatively stable at a high value as opposed to an obvious decline for the baseline case, while the total salt affected area is similar among RCPs with a relatively constant offset visible throughout the period. The results suggest a reduction in the rate of salt discharge and an increase in soil salinity with increasing severity of climate change, and there is a marginal variation of results for RCPs 4.5 and 6.0.

4. Conclusion

This study provides a rare example of applying a physically-based, fully integrated numerical model to catchment-scale water fluxes and salt transport in intermittent catchments.

MIKE SHE proved efficient in its application to an intermittent flow regime with water balance results comparable to similar models applied to the same catchment (Camporese et al., 2014; Dean et al., 2016). It was shown that calibration of K&J evapotranspiration parameters may lead to equifinality in water balance components and catchment-wide water table configuration, while the spatial distribution of ET experiences significant variability across different calibrations. Therefore, the

availability of point estimates of ET components would be useful to constrain the range of suitable solutions.

A salt balance model of the catchment was set up based on the advection–dispersion solute transport solver of MIKE SHE and observed groundwater concentrations. It was illustrated that catchment salt discharge could be reproduced by the model; however, concentration mismatch is observable for some flow events. The model also demonstrates a reasonable performance in capturing transient salinity dynamics and solute mobilization between saturated and unsaturated zones with respect to wet and dry seasons.

Projected changes in climatic data were used in a number of scenario simulations to estimate the potential impacts of future climate. Overall, a decreasing trend in salt output rate with increasing concentration of greenhouse gas emissions is expected, while, on average, the top soil will sustain relatively high salinity levels under the generally hotter and drier climate scenarios. On the contrary, under a no change scenario, a steady drop in the soil salinity is conceivable as the catchment becomes depleted of salt.

This study is one of the first attempts to establish a physically-based salinity model at the catchment scale in intermittent catchments. More complex models are required to fully account for the contributions of salts to sodicity, and thus possible alterations in soil physical properties. The results could probably be further improved by implementing a crop salt stress model to account for reduction in ET rates in saline areas.

This paper demonstrates an example of the application of MIKE SHE, or other ISSHMs, as powerful numerical tools to the management of dryland salinity. This provides insight into the potential spaces for improvement of these models for developers, as well as directions for observation efforts towards better modelling of the issue. It is worth citing that the results of this paper, particularly regarding the long-term climate change impacts, are not meant for predicting the future, but to help with the understanding of possible outcomes under the given scenarios.

Declarations of interest

None.

Acknowledgments

The experimental data were collected as part of a project initiated and funded by the Victoria Department of Economic Development, Jobs, Transport, and Resources (DEDJTR); over the years, additional support was provided by the Australian Research Council (ARC) and the National Water Commission through Program 4 (Groundwater–Vegetation–Atmosphere Interactions) of the National Centre for Groundwater Research and Training (ARC project SR0800001). E. Daly and M. Camporese acknowledge the ARC support through the Linkage Project LP140100871. E. Daly thanks the Faculty of Engineering at Monash University for supporting his Outside Study Program and the Department of Civil, Environmental and Architectural Engineering at the University of Padova, Italy, for hosting him when the manuscript was written. The Authors are grateful to the pasture landowner Marcia Field for granting access to their land. The data used in this study are available from the DEDJTR data repository by contacting P. Evan Dresel (evan.dresel@ecodev.vic.gov.au) or, alternatively, E. Daly (edoardo.daly@monash.edu). The authors also acknowledge the World Climate Research Programme's Working Group on Coupled Modelling, which is responsible for CMIP, and thank the climate modelling groups for producing and making available their model output. For CMIP, the U.S. Department of Energy's Program for Climate Model Diagnosis and Intercomparison provides coordinating support and led development of software infrastructure in partnership with the Global Organization for Earth System Science Portals.

Appendix A. Model performance metrics

Performance evaluation metrics for catchment discharge and bore water table levels for calibration and validation of the model.

Table A.1
Performance evaluation metrics for catchment discharge and bore water table levels for calibration and validation of the model.

Gauge	IoA	R^2	RMSE	ME	SDR	NSE
Calibration						
B96	0.94	0.89	0.19	0.004	0.19	
B76	0.35	0.21	0.5	−0.392	0.41	
B74	0.23	0.8	1.29	1.287	0.11	
Water discharge	0.92	0.74	0.05	0.001	0.05	0.74
Solute discharge	0.8	0.45	2.46	−0.004	2.47	0.42
Validation						
B96	0.83	0.76	0.56	0.217	0.51	
B76	0.37	0.4	0.86	−0.669	0.54	
B74	0.22	0.79	1.43	1.421	0.14	
Water discharge	0.8	0.66	0.1	−0.033	0.1	0.46
Solute discharge	0.79	0.5	3.28	−0.538	3.24	0.49

IoA: Index of Agreement; R^2: coefficient of determination; RMSE: Root Mean Square Error; ME: Mean error; SDR: Standard Deviation of Residuals; NSE: Nash–Sutcliffe Efficiency.

Appendix B. Calibrated values for ET parameters

Table B.1
ET parameter values obtained through auto-calibration with equally good model performance. The table also includes the root mean square error between the observed and simulated catchment discharge (RMSE), total ET, total evaporation (E), total transpiration (T), and ET at bores B74, B76, and B96.

Point	LAI	C1	C2	RMSE	Total ET	Total E	Total T	B74	B76	B96
1	1.01	0.34	0.4	3.24E−03	662	253	220	634	936	922
2	0.96	0.42	0.34	3.25E−03	665	220	258	652	928	890
3	1.11	0.36	0.33	3.27E−03	662	214	255	691	927	909
4	0.9	0.38	0.4	3.28E−03	662	257	222	711	936	896
5	1.13	0.34	0.37	3.29E−03	667	231	243	651	932	920
6	1.12	0.31	0.41	3.28E−03	665	253	220	711	937	902
7	1.09	0.39	0.32	3.29E−03	667	206	269	715	926	889
8	1.01	0.38	0.37	3.30E−03	666	234	245	638	932	897
9	1.13	0.3	0.39	3.30E−03	659	248	217	633	935	893
10	1.4	0.3	0.31	3.31E−03	664	198	263	652	925	907
Range	0.9	0.3	0.31	3.24E−03	659	198	217	633	925	889
	1.4	0.42	0.41	3.31E−03	667	257	269	715	937	922

Note: water balance components are given in mm (i.e., volume divided by catchment area).

Appendix C. Seasonal dynamic of salinized area

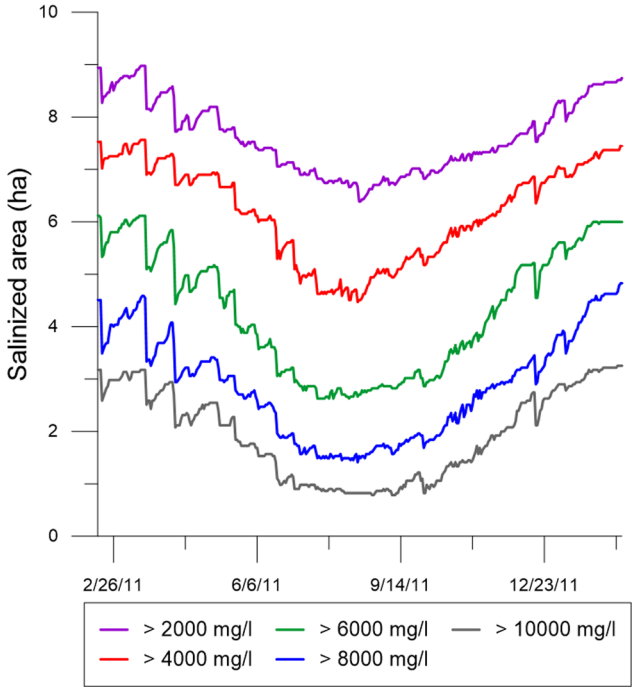

Fig. C.1. Seasonal patterns for change in salt affected area as determined per greater than threshold salinity levels. The results are related to simulations from Feb 2011 to Feb 2012.

References

Adelana, S.M., Dresel, P.E., Hekmeijer, P., Zydor, H., Webb, J.A., Reynolds, M., Ryan, M., 2015. A comparison of streamflow, salt and water balances in adjacent farmland and forest catchments in South-Western Victoria, Australia. Hydrol. Process. 29 (6), 1630–1643. https://doi.org/10.1002/hyp.10281.

Ajami, H., McCabe, M.F., Evans, J.P., 2015. Impacts of model initialization on an integrated surface water-groundwater model. Hydrol. Process. 29 (17), 3790–3801. https://doi.org/10.1002/hyp.10478.

Alaghmand, S., Beecham, S., Hassanli, A., 2014a. Impacts of vegetation cover on surface-groundwater flows and solute interactions in a semi-arid saline floodplain: a case study of the lower Murray River, Australia. Environ. Process. 1 (1), 59–71. https://doi.org/10.1007/s40710-014-0003-0.

Alaghmand, S., Beecham, S., Jolly, I.D., Holland, K., Woods, J., Hassanli, A., 2014b. Modelling the impacts of river stage manipulation on a complex river-floodplain system in a semi-arid region. Environ. Modell. Software 59, 109–126. https://doi.org/10.1016/j.envsoft.2014.05.013.

Alaghmand, S., Beecham, S., Woods, J., Holland, K., Jolly, I., Hassanli, A., Nouri, H., 2015. Injection of fresh river water into a saline floodplain aquifer as a salt interception measure in a semi-arid environment. Ecol. Eng. 75, 308–322. https://doi.org/10.1016/j.ecoleng.2014.11.014.

Alaghmand, S., Beecham, S., Woods, J., Holland, K., Jolly, I.D., Hassanli, A., Nouri, H., 2016. Quantifying the impacts of artificial flooding as a salt interception measure on a river-floodplain interaction in a semi-arid saline floodplain. Environ. Modell. Software 79, 167–183. https://doi.org/10.1016/j.envsoft.2016.02.006.

Anandhi, A., Frei, A., Pierson, D.C., Schneiderman, E.M., Zion, M.S., Lounsbury, D., Matonse, A.H., 2011. Examination of change factor methodologies for climate change impact assessment. Water Resour. Res. 47 (3). https://doi.org/10.1029/2010WR009104. w03501.

Anderies, J.M., 2005. Minimal models and agroecological policy at the regional scale: an application to salinity problems in southeastern Australia. Reg. Environ. Change 5 (1), 1–17. https://doi.org/10.1007/s10113-004-0081-z.

Barrow, C., 1992. World atlas of desertification (United nations environment programme), edited by N. Middleton and DSG Thomas. Edward arnold, London, 1992. isbn 0 340 55512 2, 89.50 (hardback), ix + 69 pp. Land Degradation & Development 3 (4), 249–249. doi: https://doi.org/10.1002/ldr.3400030407.

Bennetts, D., Webb, J., Stone, D., Hill, D., 2006. Understanding the salinisation process for

groundwater in an area of south-eastern Australia, using hydrochemical and isotopic evidence. J. Hydrol. 323 (1–4), 178–192. https://doi.org/10.1016/j.jhydrol.2005.08.023.

Brown, A.E., Zhang, L., McMahon, T.A., Western, A.W., Vertessy, R.A., 2005. A review of paired catchment studies for determining changes in water yield resulting from alterations in vegetation. J. Hydrol. 310 (1), 28–61. https://doi.org/10.1016/j.jhydrol.2004.12.010.

Camporese, M., Daly, E., Dresel, P.E., Webb, J.A., 2014. Simplified modeling of catchment-scale evapotranspiration via boundary condition switching. Adv. Water Resour. 69, 95–105. https://doi.org/10.1016/j.advwatres.2014.04.008.

Camporese, M., Daly, E., Paniconi, C., 2015. Catchment-scale Richards equation-based modeling of evapotranspiration via boundary condition switching and root water uptake schemes. Water Resour. Res. 51 (7), 5756–5771. https://doi.org/10.1002/2015WR017139.

Camporese, M., Paniconi, C., Putti, M., Orlandini, S., 2010. Surface-subsurface flow modeling with path-based runoff routing, boundary condition-based coupling, and assimilation of multisource observation data. Water Resour. Res. 46 (2). https://doi.org/10.1029/2008WR007536.

Chanson, H., 2004. Hydraulics of Open Channel Flow. Butterworth-Heinemann.

Croke, B., Jakeman, A., 2008. Use of the IHACRES rainfall-runoff model in arid and semi arid regions. In: Weather, H., Sorooshian, S., Sharma, K.D. (Eds.), Hydrological modelling in arid and semi-arid areas. Cambridge University Press, pp. 41–48. https://doi.org/10.1017/CBO9780511535734.005.

Dean, J., Camporese, M., Webb, J., Grover, S., Dresel, P., Daly, E., 2016. Water balance complexities in ephemeral catchments with different land uses: Insights from monitoring and distributed hydrologic modeling. Water Resour. Res. 52 (6), 4713–4729. https://doi.org/10.1002/2016WR018663.

Dean, J., Webb, J., Jacobsen, G., Chisari, R., Dresel, P., 2014. Biomass uptake and fire as controls on groundwater solute evolution on a southeast Australian granite: aboriginal land management hypothesis. Biogeosciences 11 (15), 4099–4114. https://doi.org/10.5194/bg-11-4099-2014.

Dean, J., Webb, J., Jacobsen, G., Chisari, R., Dresel, P., 2015. A groundwater recharge perspective on locating tree plantations within low-rainfall catchments to limit water resource losses. Hydrol. Earth Syst. Sci. 19 (2), 1107–1123. https://doi.org/10.5194/hess-19-1107-2015.

DEDJTR, Department of Economic Development, Jobs, Transport and Resources, 2017 (accessed October 10, 2017). Measuring the salinity of water. http://agriculture.vic.gov.au/agriculture/farm-management/soil-and-water/salinity/measuring-the-salinity-of-water.

DHI, 2014. MIKE SHE user manual reference guide.

Dresel, P.E., Dean, J.F., Perveen, F., Webb, J.A., Hekmeijer, P., Adelana, S.M., Daly, E., 2018. Effect of Eucalyptus plantations, geology, and precipitation variability on water resources in upland intermittent catchments. J. Hydrol. 564, 723–739. https://doi.org/10.1016/j.jhydrol.2018.07.019.

Flugel, W.-A., 1995. River salination due to dryland agriculture in the Western Cape Province, Republic of South Africa. Environ. Int. 21 (5), 679–686. https://doi.org/10.1016/0160-4120(95)00073-T.

Ghassemi, F., Jakeman, A.J., Nix, H.A., 1995. Salinisation of land and water resources: human causes, extent, management and case studies. CAB international.

Haaken, K., Deidda, G.P., Cassiani, G., Deiana, R., Putti, M., Paniconi, C., Scudeler, C., Kemna, A., 2017. Flow dynamics in hyper-saline aquifers: Hydro-geophysical monitoring and modeling. Hydrol. Earth Syst. Sci. 21 (3), 1439. https://doi.org/10.5194/hess-21-1439-2017.

Hargreaves, G.H., Samani, Z.A., 1985. Reference crop evapotranspiration from temperature. Appl. Eng. Agric. 1 (2), 96–99. https://doi.org/10.13031/2013.26773.

Hester, E.T., Hammond, B., Scott, D.T., 2016. Effects of inset floodplains and hyporheic exchange induced by in-stream structures on nitrate removal in a headwater stream. Ecol. Eng. 97, 452–464. https://doi.org/10.1016/j.ecoleng.2016.10.036.

Jiang, Y., Xu, X., Huang, Q., Huo, Z., Huang, G., 2015. Assessment of irrigation performance and water productivity in irrigated areas of the middle Heihe River basin using a distributed agro-hydrological model. Agric. Water Manag. 147, 67–81. https://doi.org/10.1016/j.agwat.2014.08.003.

Jolly, I.D., McEwan, K.L., Holland, K.L., 2008. A review of groundwater-surface water interactions in arid/semi-arid wetlands and the consequences of salinity for wetland ecology. Ecohydrology 1 (1), 43–58. https://doi.org/10.1002/eco.6.

Jolly, I.D., Williamson, D.R., Gilfedder, M., Walker, G.R., Morton, R., Robinson, G., Jones, H., Zhang, L., Dowling, T.I., Dyce, P., Nathan, R.J., Nandakumar, N., Clarke, R., McNeill, V., 2001. Historical stream salinity trends and catchment salt balances in the Murray-Darling Basin, Australia. Marine Freshwater Res. 52 (1), 53–63. https://doi.org/10.1071/MF00018.

Kollet, S., Sulis, M., Maxwell, R.M., Paniconi, C., Putti, M., Bertoldi, G., Coon, E.T., Cordano, E., Endrizzi, S., Kikinzon, E., Mouche, E., Mügler, C., Park, Y.-J., Refsgaard, J.C., Stisen, S., Sudicky, E., 2016. The integrated hydrologic model intercomparison project, ih-mip2: a second set of benchmark results to diagnose integrated hydrology and feedbacks. Water Resour. Res. 53 (1), 867–890. URL https://agupubs.onlinelibrary.wiley.com/doi/abs/10.1002/2016WR019191.

Kollet, S.J., Maxwell, R.M., 2006. Integrated surface-groundwater flow modeling: a free-surface overland flow boundary condition in a parallel groundwater flow model. Adv. Water Resour. 29 (7), 945–958. URL http://www.sciencedirect.com/science/article/pii/S0309170805002101.

Kristensen, K., Jensen, S., 1975. A model for estimating actual evapotranspiration from potential evapotranspiration. Hydrol. Res. 6 (3), 170–188. URL http://hr.iwaponline.com/content/6/3/170.

Lambers, H., 2003. Introduction, dryland salinity: a key environmental issue in southern Australia. Plant Soil 257 (2), 5–7. https://doi.org/10.1023/B:PLSO.0000003909.80658.d8.

Leblanc, M., Tweed, S., Dijk, A.V., Timbal, B., 2012. A review of historic and future hydrological changes in the Murray-Darling Basin. Global Planet. Change 80–81, 226–246. https://doi.org/10.1016/j.gloplacha.2011.10.012.

Liggett, J.E., Werner, A.D., Smerdon, B.D., Partington, D., Simmons, C.T., 2014. Fully integrated modeling of surface-subsurface solute transport and the effect of dispersion in tracer hydrograph separation. Water Resour. Res. 50 (10), 7750–7765. https://doi.org/10.1002/2013WR015040.

Long, S.A., Tachiev, G.I., Fennema, R., Cook, A.M., Sukop, M.C., Miralles-Wilhelm, F., 2015. Modeling the impact of restoration efforts on phosphorus loading and transport through Everglades National Park, FL, USA. Sci. Total Environ. 520, 81–95. https://doi.org/10.1016/j.scitotenv.2015.01.094.

Madsen, H., 2003. Parameter estimation in distributed hydrological catchment modelling using automatic calibration with multiple objectives. Adv. Water Resour. 26 (2), 205–216. https://doi.org/10.1016/S0309-1708(02)00092-1.

Marchesini, V.A., Giménez, R., Nosetto, M.D., Jobbágy, E.G., 2017. Ecohydrological transformation in the Dry Chaco and the risk of dryland salinity: Following Australia's footsteps? Ecohydrology 10 (4). https://doi.org/10.1002/eco.1822. e1822–n/a.

Maxwell, R., Condon, L., Kollet, S., 2015. A high-resolution simulation of groundwater and surface water over most of the continental US with the integrated hydrologic model ParFlow v3. Geosci. Model Dev 8 (3), 923–937. https://doi.org/10.5194/gmd-8-923-2015.

Maxwell, R.M., Putti, M., Meyerhoff, S., Delfs, J.-O., Ferguson, I.M., Ivanov, V., Kim, J., Kolditz, O., Kollet, S.J., Kumar, M., Lopez, S., Niu, J., Paniconi, C., Park, Y.-J., Phanikumar, M.S., Shen, C., Sudicky, E.A., Sulis, M., 2014. Surface-subsurface model intercomparison: a first set of benchmark results to diagnose integrated hydrology and feedbacks. Water Resour. Res. 50 (2), 1531–1549. URL https://agupubs.onlinelibrary.wiley.com/doi/abs/10.1002/2013WR013725.

McFarlane, D.J., George, R.J., Barrett-Lennard, E.G., Gilfedder, M., 2016. Salinity in Dryland Agricultural Systems: Challenges and Opportunities. Springer International Publishing, Cham, pp. 521–547. https://doi.org/10.1007/978-3-319-47928-6_19.

Niedda, M., Pirastru, M., 2014. Field investigation and modelling of coupled stream discharge and shallow water-table dynamics in a small Mediterranean catchment (Sardinia). Hydrol. Process. 28 (21), 5423–5435. https://doi.org/10.1002/hyp.10016.

Oleson, K.W., Niu, G.-Y., Yang, Z.-L., Lawrence, D.M., Thornton, P.E., Lawrence, P.J., Stöckli, R., Dickinson, R.E., Bonan, G.B., Levis, S., Dai, A., Qian, T., 2008. Improvements to the Community Land Model and their impact on the hydrological cycle. J. Geophys. Res.: Biogeosci. 113 (G1). URL https://agupubs.onlinelibrary.wiley.com/doi/abs/10.1029/2007JG000563.

Pilgrim, D., Chapman, T., Doran, D., 1988. Problems of rainfall-runoff modelling in arid and semiarid regions. Hydrol. Sci. J. 33 (4), 379–400. https://doi.org/10.1080/02626668809491261.

Queensland Department of Science, Information Technology and Innovation, 2015. Consistent Climate Scenarios User Guide. https://www.longpaddock.qld.gov.au/climateprojections/pdf/userguide.pdf.

Rengasamy, P., 2002. Transient salinity and subsoil constraints to dryland farming in Australian sodic soils: an overview. Animal Prod. Sci. 42 (3), 351–361. https://doi.org/10.1071/EA01111.

Rengasamy, P., 2006. World salinization with emphasis on Australia. J. Exp. Botany 57 (5), 1017–1023. https://doi.org/10.1093/jxb/erj108.

Richards, L.A., 1931. Capillary conduction of liquids through porous mediums. J. Appl. Phys. 1 (5), 318–333. https://doi.org/10.1063/1.1745010.

Ridley, A.M., Pannell, D.J., 2006. The role of plants and plant-based research and development in managing dryland salinity in Australia. Aust. J. Exp. Agric. 45 (11), 1341–1355. https://doi.org/10.1071/EA04153.

Runyan, C., D'Odorico, P., 2016. Global Deforestation. Cambridge University Press. https://doi.org/10.1017/CBO9781316471548.

Scudeler, C., Pangle, L., Pasetto, D., Guo-Yue, N., Volkmann, T., Paniconi, C., Putti, M., Troch, P., 2016. Multiresponse modeling of variably saturated flow and isotope tracer transport for a hillslope experiment at the Landscape Evolution Observatory. Hydrol. Earth Syst. Sci. 20 (10), 4061–4078. https://doi.org/10.5194/hess-20-4061-2016.

Shen, C., Phanikumar, M.S., 2010. A process-based, distributed hydrologic model based on a large-scale method for surface-subsurface coupling. Adv. Water Resour. 33 (12), 1524–1541. https://doi.org/10.1016/j.advwatres.2010.09.002.

Suppiah, R., Hennessy, K., Whetton, P., McInnes, K., Macadam, I., Bathols, J., Ricketts, J., Page, C., 2007. Australian climate change projections derived from simulations performed for the IPCC 4th Assessment Report. Aust. Meteorol. Mag. 56 (3), 131–152. URL http://www.bom.gov.au/amm/papers.php?year=2007.

Suweis, S., Rinaldo, A., Van der Zee, S.E.A.T.M., Daly, E., Maritan, A., Porporato, A., 2010. Stochastic modeling of soil salinity. Geophys. Res. Lett. 37 (7), l07404 https://doi.org/10.1029/2010GL042495.

Tuteja, N.K., Beale, G., Dawes, W., Vaze, J., Murphy, B., Barnett, P., Rancic, A., Evans, R., Geeves, G., Rassam, D.W., 2003. Predicting the effects of landuse change on water and salt balance-a case study of a catchment affected by dryland salinity in NSW, Australia. J. Hydrol. 283 (1), 67–90. https://doi.org/10.1016/S0022-1694(03)00236-1.

van Dijk, A.I.J.M., Beck, H.E., Crosbie, R.S., de Jeu, R.A.M., Liu, Y.Y., Podger, G.M., Timbal, B., Viney, N.R., 2013. The Millennium Drought in southeast Australia (2001–2009): natural and human causes and implications for water resources, ecosystems, economy, and society. Water Resour. Res. 49 (2), 1040–1057. https://doi.org/10.1002/wrcr.20123.

Van Genuchten, M.T., 1980. A closed-form equation for predicting the hydraulic conductivity of unsaturated soils. Soil Sci. Soc. Am. J. 44 (5), 892–898. https://doi.org/10.2136/sssaj1980.03615995004400050002x.

Vazquez, R., 2003. Effect of potential evapotranspiration estimates on effective

parameters and performance of the MIKE SHE-code applied to a medium-size catchment. J. Hydrol. 270 (3), 309–327. https://doi.org/10.1016/S0022-1694(02)00308-6.

Walker, G.R., Zhang, L., Ellis, T.W., Hatton, T.J., Petheram, C., 2002. Estimating impacts of changed land use on recharge: review of modelling and other approaches appropriate for management of dryland salinity. Hydrogeol. J. 10 (1), 68–90. https://doi.org/10.1007/s10040-001-0181-5.

Wheater, H., Sorooshian, S., Sharma, K.D., 2007. Hydrological Modelling in Arid and Semi-Arid Areas. Cambridge University Press. https://doi.org/10.1017/CBO9780511535734.

White, M., Oates, A., Barlow, T., Pelikan, M., Brown, J., Rosengren, N., Cheal, D., Sinclair, S., Sutter, G., 2003. The vegetation of north-west Victoria: a report to the Wimmera, North Central and Mallee catchment management authorities. Arthur Rylah Institute for Environmental Research, Melbourne.

Willmott, C.J., 1981. On the validation of models. Phys. Geogr. 2 (2), 184–194. URL http://www.tandfonline.com/doi/abs/10.1080/02723646.1981.10642213.

Ye, W., Bates, B., Viney, N., Sivapalan, M., Jakeman, A., 1997. Performance of conceptual rainfall-runoff models in low-yielding ephemeral catchments. Water Resour. Res. 33 (1), 153–166. https://doi.org/10.1029/96WR02840.

Ye, W., Jakeman, A.J., Young, P.C., 1998. Identification of improved rainfall-runoff models for an ephemeral low-yielding Australian catchment. Environ. Modell. Software 13 (1), 59–74. https://doi.org/10.1016/S1364-8152(98)00004-8.